CLNS 04-1883
CLEO 04-9
CLEO CONF 04-08
ICHEP04 ABS10-0771

Observation of 1^-0^- Final States from $\psi(2S)$ Decays and e^+e^- Annihilation*

N. E. Adam,[1] J. P. Alexander,[1] K. Berkelman,[1] D. G. Cassel,[1] J. E. Duboscq,[1] K. M. Ecklund,[1] R. Ehrlich,[1] L. Fields,[1] R. S. Galik,[1] L. Gibbons,[1] B. Gittelman,[1] R. Gray,[1] S. W. Gray,[1] D. L. Hartill,[1] B. K. Heltsley,[1] D. Hertz,[1] L. Hsu,[1] C. D. Jones,[1] J. Kandaswamy,[1] D. L. Kreinick,[1] V. E. Kuznetsov,[1] H. Mahlke-Krüger,[1] T. O. Meyer,[1] P. U. E. Onyisi,[1] J. R. Patterson,[1] D. Peterson,[1] J. Pivarski,[1] D. Riley,[1] J. L. Rosner,[1,†] A. Ryd,[1] A. J. Sadoff,[1] H. Schwarthoff,[1] M. R. Shepherd,[1] W. M. Sun,[1] J. G. Thayer,[1] D. Urner,[1] T. Wilksen,[1] M. Weinberger,[1] S. B. Athar,[2] P. Avery,[2] L. Breva-Newell,[2] R. Patel,[2] V. Potlia,[2] H. Stoeck,[2] J. Yelton,[2] P. Rubin,[3] B. I. Eisenstein,[4] G. D. Gollin,[4] I. Karliner,[4] D. Kim,[4] N. Lowrey,[4] P. Naik,[4] C. Sedlack,[4] M. Selen,[4] J. J. Thaler,[4] J. Williams,[4] J. Wiss,[4] K. W. Edwards,[5] D. Besson,[6] K. Y. Gao,[7] D. T. Gong,[7] Y. Kubota,[7] S. Z. Li,[7] R. Poling,[7] A. W. Scott,[7] A. Smith,[7] C. J. Stepaniak,[7] J. Urheim,[7] Z. Metreveli,[8] K. K. Seth,[8] A. Tomaradze,[8] P. Zweber,[8] J. Ernst,[9] H. Severini,[10] P. Skubic,[10] D. M. Asner,[11] S. A. Dytman,[11] S. Mehrabyan,[11] J. A. Mueller,[11] V. Savinov,[11] Z. Li,[12] A. Lopez,[12] H. Mendez,[12] J. Ramirez,[12] G. S. Huang,[13] D. H. Miller,[13] V. Pavlunin,[13] B. Sanghi,[13] E. I. Shibata,[13] I. P. J. Shipsey,[13] G. S. Adams,[14] M. Chasse,[14] J. P. Cummings,[14] I. Danko,[14] J. Napolitano,[14] D. Cronin-Hennessy,[15] C. S. Park,[15] W. Park,[15] J. B. Thayer,[15] E. H. Thorndike,[15] T. E. Coan,[16] Y. S. Gao,[16] F. Liu,[16] M. Artuso,[17] C. Boulahouache,[17] S. Blusk,[17] J. Butt,[17] E. Dambasuren,[17] O. Dorjkhaidav,[17] N. Menaa,[17] R. Mountain,[17] H. Muramatsu,[17] R. Nandakumar,[17] R. Redjimi,[17] R. Sia,[17] T. Skwarnicki,[17] S. Stone,[17] J. C. Wang,[17] K. Zhang,[17] A. H. Mahmood,[18] S. E. Csorna,[19] G. Bonvicini,[20] D. Cinabro,[20] M. Dubrovin,[20] R. A. Briere,[21] G. P. Chen,[21] T. Ferguson,[21] G. Tatishvili,[21] H. Vogel,[21] and M. E. Watkins[21]

(CLEO Collaboration)

[1] *Cornell University, Ithaca, New York 14853*
[2] *University of Florida, Gainesville, Florida 32611*
[3] *George Mason University, Fairfax, Virginia 22030*
[4] *University of Illinois, Urbana-Champaign, Illinois 61801*
[5] *Carleton University, Ottawa, Ontario, Canada K1S 5B6 and the Institute of Particle Physics, Canada*
[6] *University of Kansas, Lawrence, Kansas 66045*
[7] *University of Minnesota, Minneapolis, Minnesota 55455*
[8] *Northwestern University, Evanston, Illinois 60208*
[9] *State University of New York at Albany, Albany, New York 12222*
[10] *University of Oklahoma, Norman, Oklahoma 73019*
[11] *University of Pittsburgh, Pittsburgh, Pennsylvania 15260*
[12] *University of Puerto Rico, Mayaguez, Puerto Rico 00681*
[13] *Purdue University, West Lafayette, Indiana 47907*
[14] *Rensselaer Polytechnic Institute, Troy, New York 12180*

[15] *University of Rochester, Rochester, New York 14627*
[16] *Southern Methodist University, Dallas, Texas 75275*
[17] *Syracuse University, Syracuse, New York 13244*
[18] *University of Texas - Pan American, Edinburg, Texas 78539*
[19] *Vanderbilt University, Nashville, Tennessee 37235*
[20] *Wayne State University, Detroit, Michigan 48202*
[21] *Carnegie Mellon University, Pittsburgh, Pennsylvania 15213*
(Dated: August 1, 2004)

Abstract

Using CLEO data collected from CESR e^+e^- collisions at the $\psi(2S)$ resonance and nearby continuum at $\sqrt{s}$=3.67 GeV, we report the first significantly non-zero measurements of light vector-pseudoscalar hadron pair production (including $\rho\pi$, $\omega\pi$, $\rho\eta$, and $K^{*0}\bar{K}^0$) and the $\pi^+\pi^-\pi^0$ final state, both from $\psi(2S)$ decays and direct e^+e^- annihilation.

*Submitted to the 32$^{\rm nd}$ International Conference on High Energy Physics, August 2004, Beijing
†On leave of absence from University of Chicago.

The $\rho\pi$ puzzle poses one of the most enduring questions in strong interaction physics: why is the branching fraction for $\psi(2S) \to \rho\pi$ at least twenty [1] times smaller than expected from scaling the $J/\psi \to \rho\pi$ rate by the ratio of dilepton branching fractions? The "12% rule", a scaling conjecture generalizing this question for any decay mode, has as its underlying assumption that since charmonium decay to light hadrons must proceed through annihilation of the constituent $c\bar{c}$ into a photon or three gluons, the decay width should be proportional to the square of the $c\bar{c}$ wave function overlap at the origin. The rule's figure of merit is

$$Q_X = \frac{\mathcal{B}(\psi(2S) \to X)/\mathcal{B}(J/\psi \to X)}{\mathcal{B}(\psi(2S) \to \ell^+\ell^-)/\mathcal{B}(J/\psi \to \ell^+\ell^-)} \quad , \tag{1}$$

where $\mathcal{B}$ denotes a branching fraction and X a particular final state. Decays to dileptons also proceed via $c\bar{c}$ annihilation, and their branching fractions are well-measured [1], so their ratio makes a suitable denominator in Eq. (1). Modest deviations of Q from unity are expected [2]. In contrast to $\rho\pi$, several other channels have Q-values consistent with unity [1]. However, the $\rho\pi$ channel is not alone: significant suppressions also exist for at least one other vector-pseudoscalar (VP) channel ($K^*(892)^+K^-$) and three vector-tensor channels ($\rho a_2(1320)$, $K^*(892)\bar{K}_2^*(1430)$, and $\omega f_2(1270)$) [1, 3].

The continuing struggle to understand the pattern of Q-values has provoked many theoretical explanations. For isospin-violating (IV) modes such as $\omega\pi$ and $\rho\eta$, three-gluon mediated decay is suppressed, allowing the electromagnetic process of annihilation into a virtual photon to dominate. Whether $Q_{\rm IV} \sim 1$ remains a crucial open question. A recent review [2] of relevant theory and experiment concludes that none of the proffered theoretical explanations is satisfactory and also finds the underpinnings of the 12% rule overly simplistic.

A major impediment to addressing the puzzle in a systematic manner is the dearth of $\psi(2S)$ branching fraction measurements. Experimental progress on key VP final states has remained dormant for many years. Continuum production, $e^+e^- \to \gamma^* \to X$, which is of interest in its own right [4, 5], is expected at levels that may affect $\psi(2S)$ backgrounds and will interfere [6] with $\psi(2S)$ decay, but has not yet been measured. Using e^+e^- collision data acquired with the CLEO detector operating at the Cornell Electron Storage Ring (CESR), this Letter presents $\psi(2S)$ branching fractions and continuum cross sections for $\pi^+\pi^-\pi^0$; $\rho\pi$, $\omega\pi$, $\phi\pi$, $\rho\eta$, $\omega\eta$, $\phi\eta$, $K^{*0}(892)\bar{K}^0$, $K^{*+}(892)K^-$; $b_1(1235)\pi$. Where applicable, the inclusion of charge conjugate states is implied. We use $\rho \to \pi\pi$, $\pi^0 \to \gamma\gamma$, $\omega \to \pi^+\pi^-\pi^0$, $\phi \to K^+K^-$, $\eta \to \gamma\gamma$ and $\pi^+\pi^-\pi^0$, $K^{*0} \to K^-\pi^+$, $K^{*+} \to K^0_S\pi^+$ and $K^+\pi^0$, and $K^0_S \to \pi^+\pi^-$.

The CLEO III detector [7] features a solid angle coverage for charged and neutral particles of 93%. The charged particle tracking system, operating in a 1.0 T magnetic field along the beam axis, achieves a momentum resolution of $\sim$0.6% at $p = 1$ GeV/c. The calorimeter attains a photon energy resolution of 2.2% at $E_\gamma = 1$ GeV and 5% at 100 MeV. Two particle identification systems, one based on energy loss (dE/dx) in the drift chamber and the other a ring-imaging Cherenkov (RICH) detector, are used together to separate $K^\pm$ from $\pi^\pm$. The combined dE/dx-RICH particle identification procedure has efficiencies of exceeding 90% and misdentification rates below 5% for both $\pi^\pm$ and $K^\pm$.

Half of the $\psi(2S)$ data and all the $\sqrt{s}$=3.67 GeV data were taken after a transition to the CLEO-c [8] detector configuration, in which CLEO III's silicon-strip vertex detector was replaced with a six-layer all-stereo drift chamber. The two detector configurations correspond to different accelerator lattices: the former with a single wiggler magnet and a center-of-mass energy spread of 1.5 MeV, the latter (CESR-c [8]) with six wiggler magnets and an energy spread of 2.3 MeV.

The integrated luminosity ($\mathcal{L}$) of the datasets was measured using $\gamma\gamma$ events in the calorimeter [9]. Event counts were normalized with a Monte Carlo (MC) simulation based on the Babayaga [10] event generator combined with GEANT-based [11] detector modeling. The datasets have $\mathcal{L}$=5.46 pb^{-1} on the peak of the $\psi(2S)$ (2.57 pb^{-1} for CLEO III, 2.89 pb^{-1} for CLEO-c) and 20.46 pb^{-1} at $\sqrt{s}$=3.67 GeV (all CLEO-c). The scale factor applicable to continuum yields in order to normalize them to $\psi(2S)$ data, $f = 0.260 \pm 0.004$, includes a 2.6% correction to the $\mathcal{L}$ ratio to scale it by $1/s^3$ [5]; the error includes both the relative luminosity and form factor s-dependence uncertainties. We also correct each final state's f for small efficiency differences between the $\psi(2S)$ and continuum samples caused by detector configuration.

We base our event selection on charged particles reconstructed in the tracking system and photon candidates in the CsI calorimeter. Energy and momentum conservation is required of the reconstructed hadrons, which have momenta p_i and total energy $E_{\rm vis}$. We demand $0.98 < E_{\rm vis}/\sqrt{s} < 1.015$ and $||p_1| - |p_2||/\sqrt{s} < 0.02$ (for $\pi^+\pi^-\pi^0$, $p_1 = p_{\pi^0}$ and $p_2 = p_{\pi^+} + p_{\pi^-}$), which together suppress backgrounds with missing energy or incorrect mass assignments. The experimental resolutions are smaller than 1% in scaled energy and 2% in scaled momentum difference. In order to suppress hadronic transitions to J/ψ, we reject events in which any of the following fall within 3.05-3.15 GeV: the invariant mass of the two highest momentum tracks; or the recoil mass from the lowest momentum single π^0, $\pi^0\pi^0$ pair, or $\pi^+\pi^-$ pair. Feeddown from $\pi^0\pi^0 J/\psi$, $J/\psi \to \mu^+\mu^-$ into $\pi^+\pi^-\pi^0$, $\rho^+\pi^-$, or $(K^+\pi^0)K^-$ is additionally suppressed by requiring $M(\mu^+\mu^-) < 3.05$ GeV for those channels.

MC studies were used to determine invariant mass windows for intermediate particle decay products. To avoid contamination from $\omega f_2(1270)$ and $\omega f_0(600)$ [12] in $b_1\pi$, we exclude $M_{\pi\pi}$ <1.5 GeV. Similarly, $\rho\eta$ candidates with low mass $\eta\pi^\pm$ states are avoided with $M(\eta\pi^\pm)_{\rm min} > 1.4$ GeV. For $\pi^0 \to \gamma\gamma$, $\eta \to \gamma\gamma$, and $K^0_S \to \pi^+\pi^-$ candidates we use kinematically constrained fits of the decay products to the parent masses. Fake π^0 and η mesons are suppressed with lateral shower profile restrictions and by requiring that their decays to $\gamma\gamma$ not be too asymmetric.

For $\pi^+\pi^-\pi^0$, $\rho^+\pi^-$, and $\rho\eta$ ($\phi\eta$), one of the two charged particles must be positively identified as a $\pi^\pm$ ($K^\pm$), but neither can be positively identified as a $K^\pm$ ($\pi^\pm$). Charged kaons in K^*K must be identified as such, and any $\pi^\pm$ candidate must not be identified as $K^\pm$. Charged particles must not be identified as electrons using criteria based on momentum, calorimeter energy deposition, and dE/dx. The softer charged particle in two-track modes must have $p < 0.425 \times \sqrt{s}$. Both tracks in two-track modes must satisfy $|\cos\theta| < 0.83$, where θ is the polar angle with respect to the e^+ direction.

The efficiency ϵ for each final state is the average obtained from MC simulations [11] of both detector configurations. The VP modes are generated with angular distribution $(1 + \cos^2\theta)$ [5], $b_1\pi$ flat in $\cos\theta$, and $\pi^+\pi^-\pi^0$ as in ω decay. We assume $\mathcal{B}(b_1 \to \omega\pi)$=100%.

Event totals and efficiencies are shown in Table I and kinematic distributions in Figs. 1-4. Background contamination from other $\psi(2S)$ decays is determined from sidebands neighboring the signal windows in π^0, η, ω, ϕ, K^0_S, K^*, and b_1 candidate mass distributions. The sideband yields from the $\psi(2S)$ sample are decremented by the corresponding number of scaled continuum events (because scaled continuum events inside the signal window are subtracted separately) and by the small residual signal contributions expected, and then scaled to match the signal window size.

We normalize the corrected event totals to the number of $\psi(2S) \to \pi^+\pi^- J/\psi$, $J/\psi \to \mu^+\mu^-$ decays. Requiring that the $\mu^\pm$ candidates have $|\cos\theta| < 0.83$, the invariant mass

recoiling against the $\pi^+\pi^-$ pair be consistent with J/ψ production ($M_{\rm recoil}$=3.08-3.11 GeV), and imposing energy-momentum conservation, 2.88×10^4 events are found with ϵ=42.7%. Excellent agreement between data and MC is observed in important kinematic and angular distributions, three of which are shown in Fig. 5. The MC events were generated [13] with J/ψ decay radiation [14] and the $\pi^+\pi^-$ pair in a pure relative S-wave configuration, both with respect to each other, and, as a pair, to the J/ψ. The total number of such events produced is $(6.75 \pm 0.12) \times 10^4$, where the error accounts for data and MC statistics (0.7%) and for uncertainties in trigger efficiency (0.5%) and angular distributions (1.5%).

Table II shows the final results, neglecting effects of interference with continuum production. Statistical errors shown correspond to 68% confidence level (CL) and upper limits to 90% CL. The CL that any mean signal combined with estimated backgrounds would exceed or equal the observed event count is computed from trials in which Poisson fluctuations of the observed $\psi(2S)$, continuum, and cross-feed contributions are all simulated. Values of Q are computed for each mode based on $\mathcal{B}(\psi(2S) \to \pi^+\pi^- J/\psi) = 0.323 \pm 0.013$ and other branching fractions from Ref. [1], except for $\mathcal{B}(J/\psi \to \pi^+\pi^-\pi^0)$ [15]. Born-level cross sections at $\sqrt{s}$=3.67 GeV are also given and include an upward adjustment of 20% to account for initial state radiation [10]. The systematic errors on branching fraction ratios share common contributions from the number of $\psi(2S) \to \pi^+\pi^- J/\psi$, $J/\psi \to \mu^+\mu^-$ decays (1.7%), uncertainty in f (1.5%), trigger efficiency (1%), and electron veto (1%). Other sources vary by channel, including cross-feed adjustments (50% of each subtraction), MC statistics (2%), accuracy of MC-generated polar angle and mass distributions (5% for $b_1\pi$, 14% for $\pi^+\pi^-\pi^0$), and detector performance modeling quality: charged particle tracking (1% per track), π^0, η and K^0_S finding (2% per π^0 or η, 5% per K^0_S), $\pi^\pm/K^\pm$ identification (3% per identified π/K), and mass resolutions (2%). Cross section systematic errors include the above contributions, substituting an uncertainty in $\mathcal{L}$ (3%) for the normalization error and accounting for uncertainties in the effects of initial and final state radiation (7%). Except for $b_1\pi$ and $\pi^+\pi^-\pi^0$, statistical errors dominate.

We observe signals for several modes in both $\psi(2S)$ and continuum datasets. The $\psi(2S)$ results in Table II are consistent with previous measurements [1], where available. Unlike other VP channels, the IV modes $\omega\pi$ and $\rho\eta$ are not strongly suppressed with respect to the 12% rule, an important new piece of the $\rho\pi$ puzzle. The ratio $\mathcal{B}(\psi(2S) \to K^{*+}K^-)/\mathcal{B}(\psi(2S) \to K^{*0}\bar{K}^0) = 0.12^{+0.11}_{-0.09}$ is found to be much smaller than the equivalent ratio for J/ψ decays, 1.19 ± 0.15 [1]. Fig. 4 shows that $\psi(2S) \to \pi^+\pi^-\pi^0$ decays have not only a distinct $\rho\pi$ component above the continuum contribution, but, unlike $J/\psi \to \pi^+\pi^-\pi^0$ [15], which is dominated by $\rho\pi$, also feature a much larger cluster of events near the center of the Dalitz plot. The $\rho\pi$ results reported here do not account for any cross-feed from the non-$\rho\pi$ component due to its uncertain source and shape. If five events inside the ρ mass window were attributed to the higher mass structure, the $\rho\pi$ branching fraction would decrease by a quarter and its significance by one unit.

With the striking exception of $K^{*0}\bar{K}^0$, VP continuum cross sections are consistent with Born-level calculations [6, 16] and the SU(3) expectation [17] for a mixing angle of $\theta_p = -19.5^\circ$, $\omega\pi : \rho\eta : K^{*0}\bar{K}^0 : \rho\pi : \phi\eta : K^{*+}K^- : \omega\eta : \phi\pi = 1 : 2/3 : 4/9 : 1/3 : 4/27 : 1/9 : 2/27 : 0$. A least-squares fit for the common unit of cross section, excluding $K^{*0}\bar{K}^0$, yields $\sigma(\omega\pi) = 16.5 \pm 2.2$ pb with $\chi^2 = 5.5$ for 6 d.o.f.; $\sigma(K^{*0}\bar{K}^0)$ exceeds $\frac{4}{9}\sigma(\omega\pi)$ by 3.2 standard deviations. The above θ_p value approximately describes η–η' mixing. Variations in θ_p of $\pm 10^\circ$ induce changes of $^{+0.7}_{-1.2}$ pb in $\sigma(\omega\pi)$.

In summary, we have presented first evidence for $\psi(2S)$ decays to $\pi^+\pi^-\pi^0$, $\rho\pi$, $\omega\pi$, $\rho\eta$,

and $K^{*0}\bar{K}^0$. Measurements for several other VP channels are also given. The results suggest that, for VP final states, $\psi(2S)$ decays through three gluons are severely suppressed with respect to the 12% rule and the corresponding electromagnetic processes are not. The decay $\psi(2S) \to \pi^+\pi^-\pi^0$ exhibits a $\rho \to \pi\pi$ signal but has a much larger component at higher $\pi\pi$ mass. Continuum e^+e^- cross sections for these final states are presented for the first time.

We gratefully acknowledge the effort of the CESR staff in providing us with excellent luminosity and running conditions. This work was supported by the National Science Foundation, the U.S. Department of Energy, the Research Corporation, and the Texas Advanced Research Program.

---

[1] Particle Data Group, S. Eidelman *et al.*, Phys. Lett. B **592**, 1 (2004).
[2] Y.F. Gu and X.H. Li, Phys. Rev. D **63**, 114019 (2001).
[3] BES Collaboration, J.Z. Bai *et al.*, Phys. Rev. D **69** 072001 (2004).
[4] P. Wang, C.Z. Yuan, and X.H. Mo, Phys. Rev. D **69**, 057502 (2004).
[5] S.J. Brodsky and G.P. Lepage, Phys. Rev. D **24**, 2848 (1981).
[6] P. Wang, C.Z. Yuan, and X.H. Mo, Phys. Lett. **B574**, 41 (2003).
[7] CLEO Collaboration, Y. Kubota *et al.*, Nucl. Instrum. Methods Phys. Res., Sect. A **320**, 66 (1992); D. Peterson *et al.*, Nucl. Instrum. Methods Phys. Res., Sect. A **478**, 142 (2002); M. Artuso *et al.*, Nucl. Instrum. Methods Phys. Res., Sect. A **502**, 91 (2003).
[8] CLEO-c/CESR-c Taskforces & CLEO-c Collaboration, Cornell LEPP preprint CLNS 01/1742 (2001).
[9] CLEO Collaboration, G. Crawford *et al.*, Nucl. Instrum. Methods Phys. Res., Sect. A **345**, 429 (1992).
[10] C.M. Carloni Calame *et al.*, hep-ph/0312014 [in Proceedings of the Workshop on Hadronic Cross Section at Low Energy (SIGHAD03), Pisa, Italy, 2003 (to be published)].
[11] R. Brun *et al.*, GEANT 3.21, CERN Program Library Long Writeup W5013 (1993), unpublished.
[12] BES Collaboration, J.Z. Bai *et al.*, Phys. Rev. D **69**, 072001 (2004).
[13] D.J. Lange, Nucl. Instrum. Methods Phys. Res., Sect. A **462**, 152 (2001).
[14] E. Barberio and Z. Was, Comput. Phys. Commun. **79**, 291 (1994).
[15] BES Collaboration, J.Z. Bai *et al.*, Phys. Lett. **B591**, 42 (2004).
[16] P. Wang, X.H. Mo, and C.Z. Yuan, Phys. Lett. **B557**, 192 (2003).
[17] H.E. Haber and J. Perrier, Phys. Rev. D **32**, 2961 (1985); L. Kopke and N. Wermes, Phys. Rep. **174**, 67 (1989).

TABLE I: For each mode: the efficiency, ϵ; for $\sqrt{s}$=3.67 GeV data, the number of events, N_c, and background from sidebands, N_{cb}; for ψ(2S) data, the number of events, N_{2S}, the estimated continuum background, fN_c, and background from other $\psi(2S)$ decays, N_b; and the statistical significance S of the $\psi(2S)$ signal in units of a Gaussian standard deviation.

Mode	ϵ(%)	N_c	N_{cb}	N_{2S}	fN_c	N_b	S
$\pi^+\pi^-\pi^0$	30.6	85	14	217	21.7	2.3	>6
$\rho^0\pi^0$	30.8	21	4	15	5.5	0	3.0
$\rho^+\pi^-$	26.9	26	2	20	6.8	3.2	2.5
$\rho\pi$	28.2	47	6	35	12.3	3.2	3.7
$\omega\pi$	18.3	55	9	31	13.9	1.9	3.1
$\phi\pi$	15.0	3	1	1	0.8	0.7	<1
$\rho\eta$	19.5	38	3	28	9.8	0	4.2
$\omega\eta$	9.4	3	0	1	0.7	1.5	<1
$\phi\eta$	8.8	3	0	9	0.8	2.4	2.1
$K^{*0}\bar{K}^0$	8.1	36	2	35	9.5	0.5	5.2
$K^{*+}K^-$	15.5	4	2	10	1.1	3.3	2.0
$b_1^0\pi^0$	5.9	5	3	54	1.3	10.0	>6
$b_1^+\pi^-$	12.2	17	3	226	4.3	62.0	>6
$b_1\pi$	10.1	22	6	280	5.6	72.0	>6

TABLE II: For each final state X: the ratio $R = \mathcal{B}(\psi(2S) \to X)/\mathcal{B}(\psi(2S) \to \pi^+\pi^- J/\psi,\ J/\psi \to \mu^+\mu^-)$, with statistical (68% CL) and systematic errors; the upper limit (90% CL), UL, for R; Q from Eq. (1); and σ, the $e^+e^- \to X$ Born-level cross section at $\sqrt{s}$=3.67 GeV.

Mode	R (10^{-4})	UL (10^{-4})	Q (10^{-2})	σ (pb)
$\pi^+\pi^-\pi^0$	$93^{+8}_{-7} \pm 14$	119	6.6±1.2	$13.1^{+2.0}_{-1.8} \pm 3.0$
$\rho^0\pi^0$	$4.7^{+2.3}_{-2.0} \pm 0.3$	8	1.7±0.9	$3.2^{+1.1}_{-0.9} \pm 0.5$
$\rho^+\pi^-$	$5.5^{+3.3}_{-2.7} \pm 0.7$	11	1.0±0.6	$5.2^{+1.4}_{-1.1} \pm 0.5$
$\rho\pi$	$10.4^{+3.9}_{-3.3} \pm 0.8$	17	1.2±0.5	$8.3^{+1.7}_{-1.4} \pm 1.2$
$\omega\pi$	$12.3^{+5.7}_{-4.7} \pm 1.1$	22	44±22	$14.2^{+2.7}_{-2.4} \pm 2.0$
$\phi\pi$	–	3	–	$0.8^{+1.3}_{-0.6} \pm 0.1$
$\rho\eta$	$14.0^{+4.8}_{-4.3} \pm 1.0$	22	109±41	$10.2^{+2.2}_{-1.9} \pm 1.6$
$\omega\eta$	–	5	<5.5	$1.8^{+1.7}_{-0.9} \pm 0.2$
$\phi\eta$	$9.7^{+7.7}_{-5.2} \pm 2.1$	23	22±18	$2.0^{+2.0}_{-1.1} \pm 0.2$
$K^{*0}\bar{K}^0$	$46^{+13}_{-11} \pm 4$	69	16±5	$24.6^{+5.1}_{-4.4} \pm 3.0$
$K^{*+}K^-$	$5.4^{+4.6}_{-3.2} \pm 1.3$	14	1.6±1.5	$0.8^{+1.4}_{-0.6} \pm 0.8$
$b_1^0\pi^0$	$108^{+23}_{-20} \pm 15$	157	70±26	$1.9^{+3.9}_{-1.7} \pm 1.4$
$b_1^+\pi^-$	$194 \pm 21 \pm 39$	266	97±28	$6.4^{+2.5}_{-2.0} \pm 1.0$
$b_1\pi$	$298^{+29}_{-28} \pm 57$	399	84±22	$8.9^{+3.5}_{-2.9} \pm 1.9$

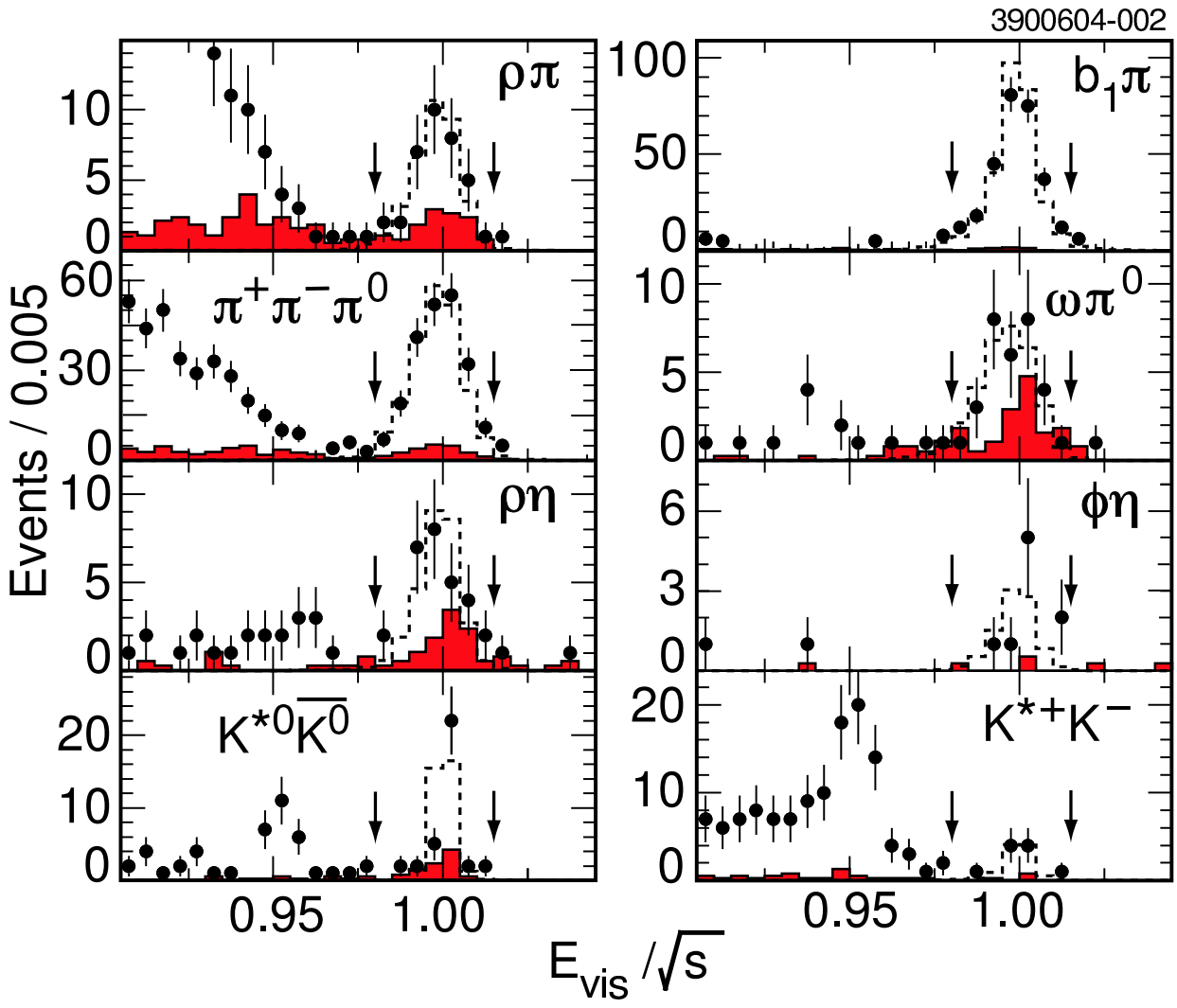

FIG. 1: Distributions of scaled visible energy, $E_{\rm vis}/\sqrt{s}$, for labeled final states. Plots for $\rho\pi$ and $b_1\pi$ sum over the charged and neutral states. Histogram entries are shown for $\psi(2S)$ data (points with error bars), scaled continuum (solid), and MC (dashed) with arbitrary normalization. The vertical arrows mark ends of signal selection ranges.

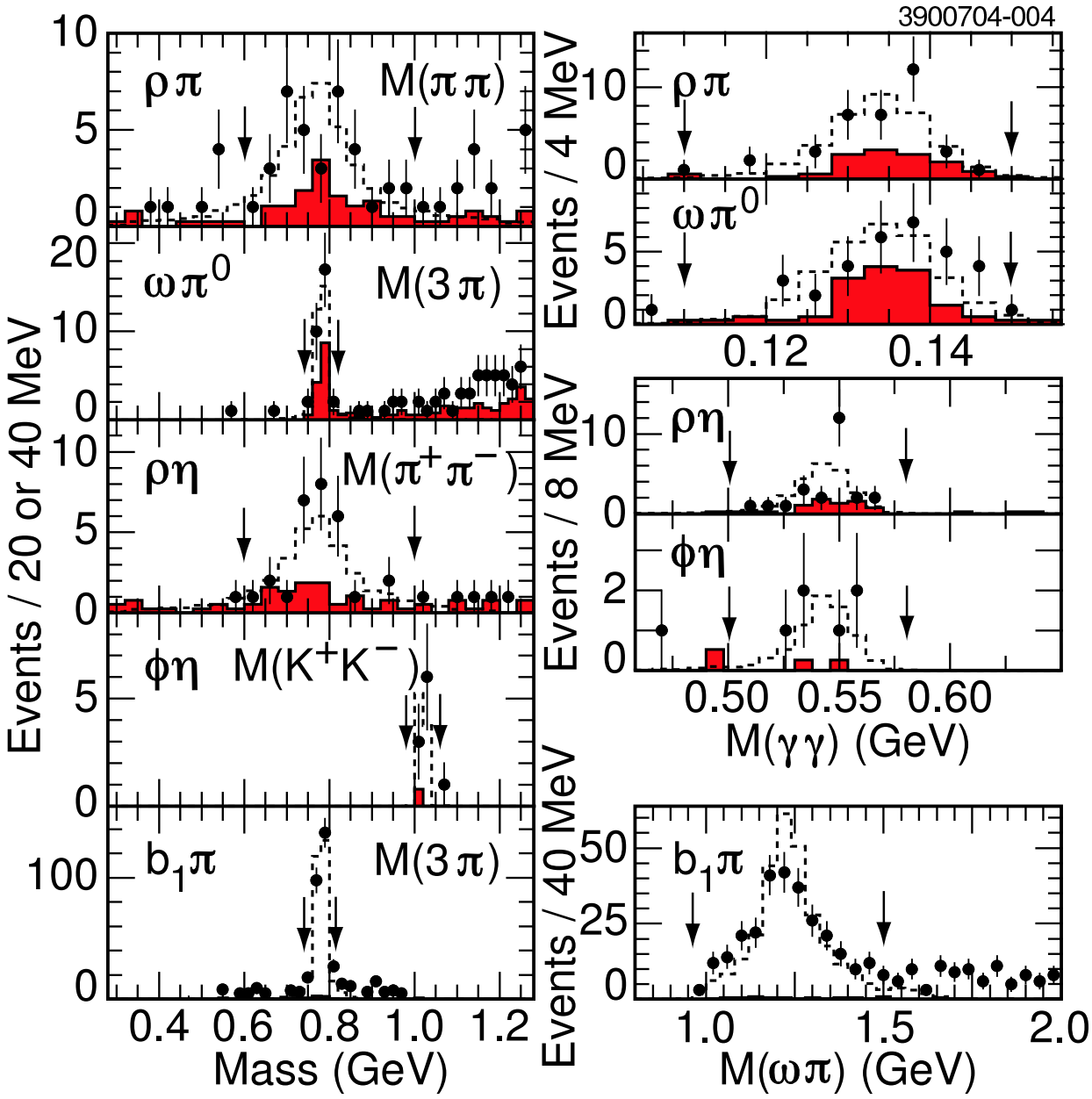

FIG. 2: Invariant mass distributions relevant to the final states indicated, one entry per event. Symbols are defined in Fig. 1.

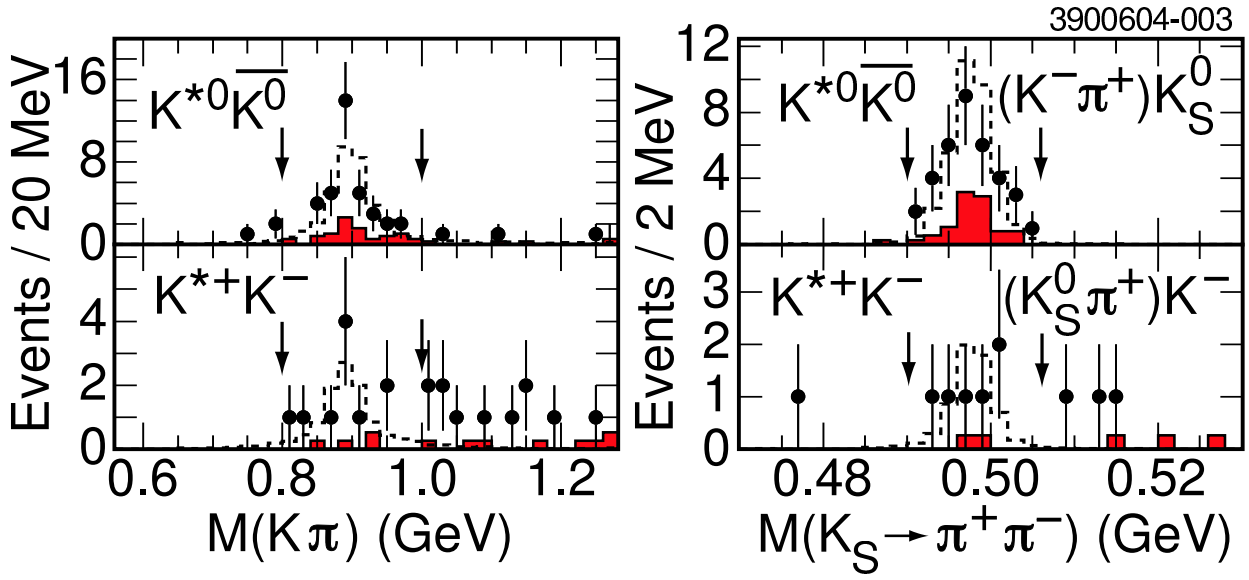

FIG. 3: Invariant masses for the $K^*(892)$ (left) and K^0_S (right) candidates, one entry per event, for the final states indicated. Symbols are defined in Fig. 1.

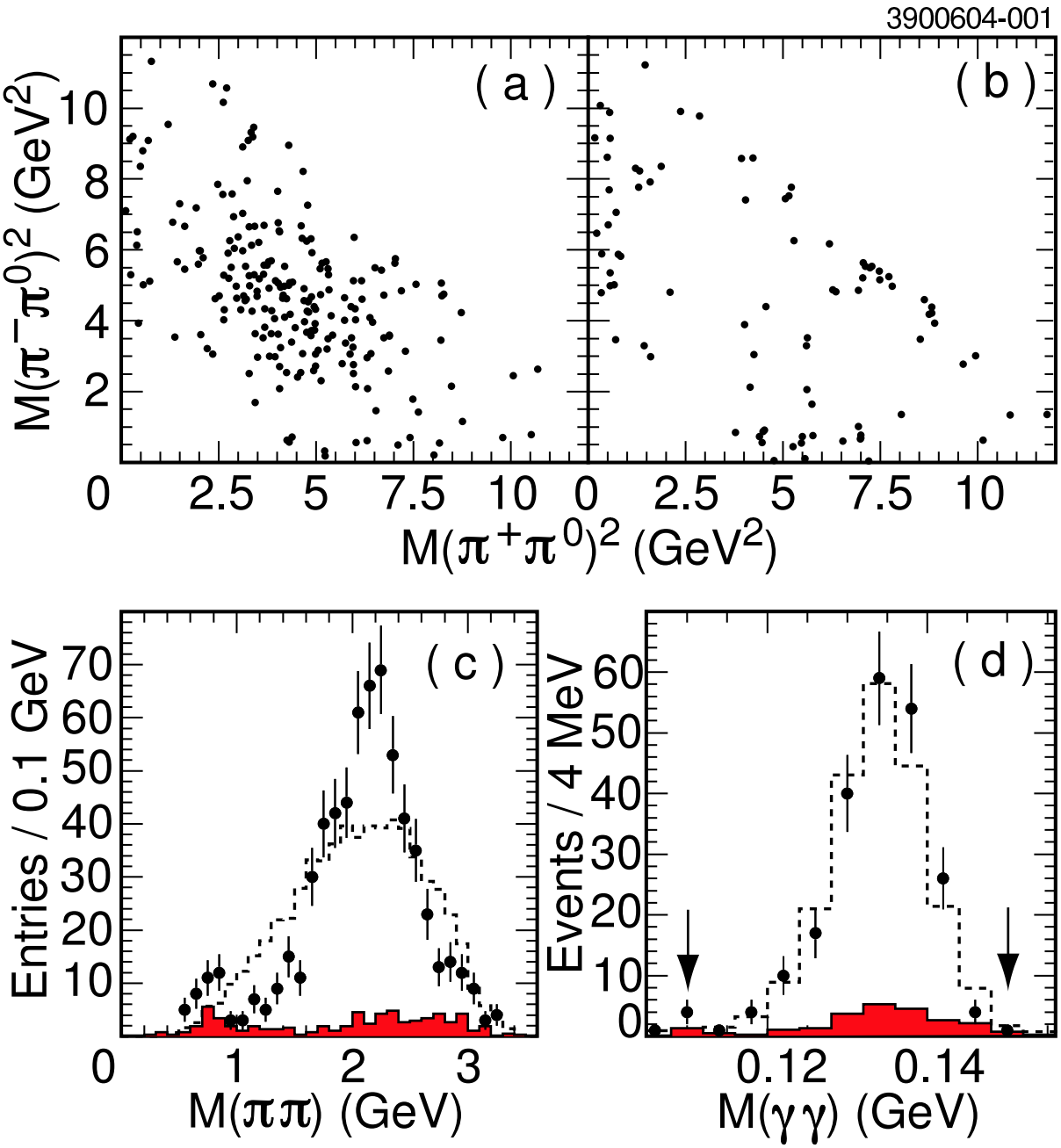

FIG. 4: Distributions for the $\pi^+\pi^-\pi^0$ final state: the Dalitz plots for (a) $\psi(2S)$ and (b) continuum data; (c) the $\pi^+\pi^-$, $\pi^+\pi^0$, and $\pi^-\pi^0$ mass combinations (3 entries/event), and (d) the $\gamma\gamma$ mass. Symbols are defined in Fig. 1.

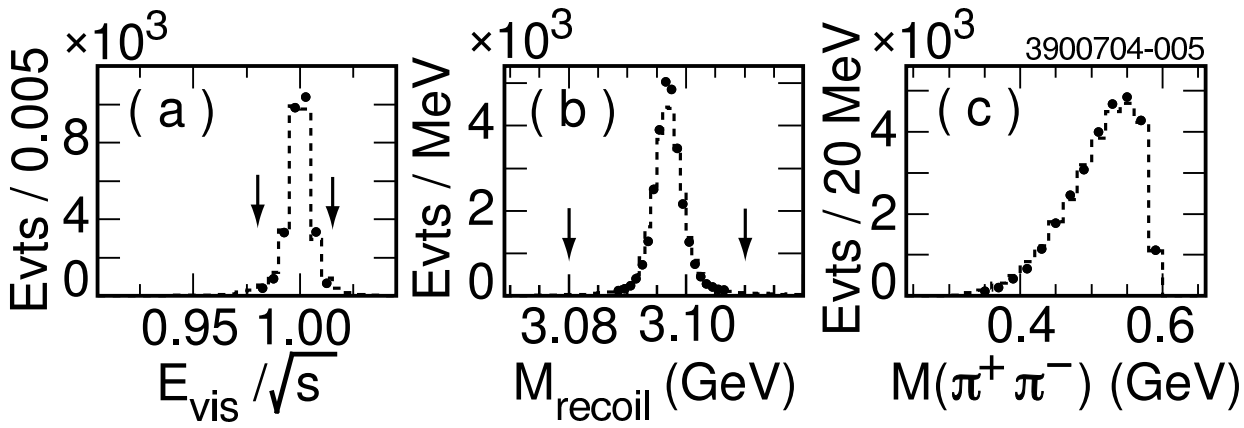

FIG. 5: Distributions for the $\pi^+\pi^- J/\psi$, $J/\psi \to \mu^+\mu^-$ final state, showing (a) $E_{\rm vis}/\sqrt{s}$, (b) $M_{\rm recoil}$, and (c) $M_{\pi^+\pi^-}$. Symbols are defined in Fig. 1.